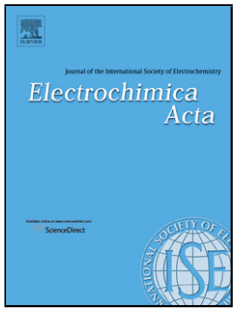

Title: Supercapacitors based on two dimensional VO_2 nanosheet electrodes in organic gel electrolyte

Author: R.B. Rakhi D.H. Nagaraju Pierre Beaujuge H.N. Alshareef

PII: S0013-4686(16)32213-7
DOI: http://dx.doi.org/doi:10.1016/j.electacta.2016.10.109
Reference: EA 28197

To appear in: *Electrochimica Acta*

Received date: 31-8-2016
Revised date: 7-10-2016
Accepted date: 17-10-2016

Please cite this article as: R.B.Rakhi, D.H.Nagaraju, Pierre Beaujuge, H.N.Alshareef, Supercapacitors based on two dimensional VO2 nanosheet electrodes in organic gel electrolyte, Electrochimica Acta http://dx.doi.org/10.1016/j.electacta.2016.10.109

Supercapacitors based on two dimensional VO_2 nanosheet electrodes in organic gel electrolyte

R. B. Rakhi [a,b,†], D. H. Nagaraju [a, †], Pierre Beaujuge[a] ,and H. N. Alshareef [a,*]

[a] Materials Science and Engineering, King Abdullah University of Science & Technology (KAUST), Thuwal 23955-6900, Saudi Arabia
[b] Chemical Sciences and Technology division, CSIR- National Institute of Interdisciplinary Sciences (CSIR-NIIST), Thiruvananthapuram, Kerala, India, 695019

*Corresponding author: husam.alshareef@kaust.edu.sa

[†] These authors contributed equally to this work.

Graphical Abstract

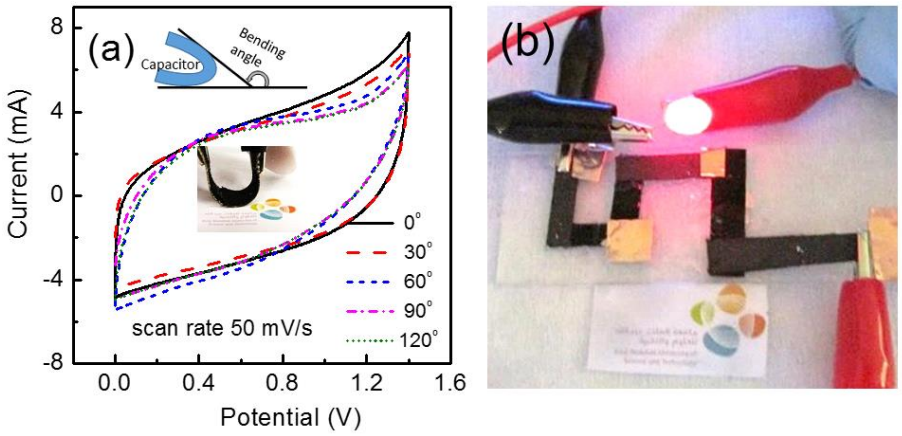

(a) CVs of solid state device measured at different angles (inset shows the schematic for the measurement of the bending angles and the optical image of the flexible supercapacitor device). (b) Optical images displaying lighting up of an LED using three flexible supercapacitors connected in series.

Highlights

- Synthesis of 2D VO_2 nanosheets by hydrothermal reduction of V_2O_5 nanopowder.
- A specific capacitance of 405 F g^{-1} in organic electrolyte at 1 A g^{-1}.
- An energy density of 46 Wh kg^{-1} at 1 Ag^{-1} for VO_2 based symmetric capacitor.
- Fabrication of all solid state flexible supercapacitors.
- Series combination of three solid state capacitors lighting up an LED for 1 minute.

ABSTRACT

VO_2 is a low band-gap semiconductor with relatively high conductivity among transition metal oxides, which makes it an interesting material for supercapacitor electrode applications. The performance of VO_2 as supercapacitor electrode in organic electrolytes has never been reported before. Herein, two-dimensional nanosheets of VO_2 are prepared by the simultaneous solution reduction and exfoliation from bulk V_2O_5 powder by hydrothermal method. A specific capacitance of 405 Fg^{-1} is achieved for VO_2 based supercapacitor in an organic electrolyte, in three electrode configuration. The symmetric capacitor based on VO_2 nanosheet electrodes and the liquid organic electrolyte exhibits an energy density of 46 Wh kg^{-1} at a power density of 1.4 kW kg^{-1} at a constant current density of 1 Ag^{-1}. Furthermore, flexible solid-state supercapacitors are fabricated using same electrode material and Alumina-silica based gel electrolyte. The solid-state device delivers a specific capacitance of 145 Fg^{-1} and a device capacitance of 36 Fg^{-1} at a discharge current density of 1 Ag^{-1}. Series combination of three solid state capacitors is capable of lighting up a red LED for more than 1 minute.

KEYWORDS

VO_2 nanosheets, Flexible, supercapacitor, Energy density, specific capacitance

1. Introduction

Inorganic graphene-like 2D materials with single or few layers have received considerable research interest recently [1-4], as these materials show distinctive physical and electrical properties, which makes them potentially useful for a variety of new applications [5-7]. One of the unique properties of ultrathin inorganic 2D nanosheets is their large surface area and their ability to undergo redox reactions efficiently, which makes them candidates for fabricating high energy density storage devices[8, 9]. Supercapacitors are high power devices that can store and deliver energy much quicker than the batteries, but they do have lower in energy densities [10-12]. To increase the energy density of supercapacitors different nanostructured materials have been investigated including redox polymers and oxides.[13-21] Although, higher energy densities have been achieved with nanostructured materials, this has often been at the expense of modest power density and cycling stability. The approach to improving the energy storage performance of pseudocapacitors should aim at reducing the ion diffusion path length and increasing the electronic conductivity as well as the surface area of the active material. Since the ionic diffusion in 2D materials is high,[22] developing a thin 2D inorganic material could result in high energy density and power density supercapacitors. The 2D metal oxides such as V_2O_5 and MoO_3 etc. have been utilized as supercapacitor electrode materials.[23-48] Among all these, vanadium oxide is gaining considerable research interest due to its ability to exist in variable oxidation states (e.g., V_2O_5, V_2O_3, and V_4O_7) [38-49]. The electronic structure, charge density, transport properties, oxidation

state and phase transitions of different vanadium oxides are expected to vary with the composition. Among the oxides of vanadium, V_2O_5 has been quite extensively investigated for energy storage applications.[50-52] On the other hand, VO_2 is an exciting phase having a low band gap of 0.7 eV, which changes monoclinic to tetragonal structure reversibly at about 68 °C and undergoes semiconductor-to-metal transition.

There are few reports of VO_2 as a supercapacitor electrode material.[53-59] Pan *et al.* have reported the conductivity of VO_2 can be enhanced by treating with hydrogen and hence supercapacitor performance[54]. At a constant current density of 1 Ag^{-1}, the specific discharge capacitance and specific energy density of hydrogen treated VO_2 was stabilized at around 300 Fg^{-1} and 17 Wh kg^{-1} respectively, which was nearly four times higher than that of pristineVO_2. This remarkable enhancement in the performance was attributed to the reduction of VO_2 resistance by nearly three orders of magnitude through H_2 treatment [54]. Zhao *et al.* have utilized the porous hierarchical VOx@carbon composites[56]. Zhao *et al.* have formed of VO_2-reduced graphene oxide composite[60]. Recently, Wang *et al.* prepared the hierarchical network framework graphene/VO_2 nanobelt composite hydrogels which exhibited a maximum energy density of 21.3 Wh kg^{-1} at a constant current density of 1 Ag^{-1} [58]. However, to the best of our knowledge, no reports are available on the electrochemical performance of VO_2 in an organic electrolyte or on flexible solid state capacitors based on VO_2 with organic gel electrolyte.

In this study, we demonstrate a process for the simultaneous reduction and exfoliation of bulk V_2O_5 powder into an assembly of 2D VO_2 nanosheets by hydrothermal method. By optimizing process conditions and choosing the appropriate hydrophilic binder, we could achieve a specific capacitance of 217 Fg^{-1} at a scan rate of 5 mV s^{-1} for VO_2 based symmetric capacitor in a propylene carbonate (PC) based organic electrolyte. Symmetric supercapacitor displays an energy density of

46 Wh kg^{-1} at a power density of 1.4 kW kg^{-1} and a constant current density of 1 Ag^{-1}. The flexible solid-state supercapacitor fabricated using VO_2 electrodes and gel organic electrolyte could deliver a specific capacitance of 145 Fg^{-1} and a gravimetric capacitance of 36 Fg^{-1} at a discharge current density of 1 Ag^{-1}.

2. Experimental

2.1 Chemicals

Ammonium metavanadate (NH_4VO_3), Hydrogen peroxide, Oxalic acid ($H_2C_2O_4$), Propylene Carbonate ($C_4H_6O_3$), Lithium perchlorate ($LiClO_4$), Polytetrafluoroethylene (PTFE), Sodium Carboxymethylcellulose (CMC), ethanol (C_2H_5OH), Fumed Silica (Aldrich) were used without further purification.

2.2 Synthesis of VO_2 2D nanosheets from V_2O_5 powder

Ammonium metavanadate powder was heated to 450 °C in air for two hours in a tube furnace at a heating rate of 10 °C per minute to obtain orange-red color V_2O_5 powder. The 0.25 g of V_2O_5 powder was dissolved in 20 ml of water using 30% H_2O_2 and stirred for 30 minutes. To this, 1g of oxalic acid was added and stirred for additional 30 minutes. The resulting dark orange-red colored solution was transferred into Teflon hydrothermal reaction autoclaves and heated to 180 °C for 24 hours. The resulting greenish black colored gel was centrifuged and washed several times with water followed by ethanol and dried at room temperature.

2.3 Instrumentation

Morphology of VO_2 was characterized by field emission scanning electron microscope (FE-SEM, FEI, Nova Nano) and transmission electron microscope (TEM, JEOL 2100F). The X-ray diffraction (XRD) was performed using Bruker diffractometer (CuKα), Brunauer-Emmett-

Teller (BET) surface area measurement was performed by using NOVA 3200e system. The VO_2 sample was degassed at 373 K under vacuum for 12 h before BET surface area measurements. Classical three-electrode configuration was used for the electrochemical characterization, consists of VO_2 modified carbon paper as a working electrode, Ag/Ag^+ as a reference electrode and Pt wire as a counter electrode. Coin type device was fabricated in symmetric cell configuration using two VO_2 electrodes of identical masses (1 mg each) with 1 M $LiClO_4$ in propylene carbonate as a liquid electrolyte and a separator.

2.4 Electrochemical Characterization

The electrodes were prepared by mixing the 85% of VO_2 with 10% weight of acetylene black and 5% binder CMC in 20 ml of water and sonicated for 30 minutes to obtain a stable dispersion solution. The dispersed solution was drop cast onto the carbon paper and dried in the oven at 50 °c for 12 hours.

The gel electrolyte was prepared by dissolving the fumed silica in a minimum quantity of propylene carbonate solution containing 1M $LiClO_4$. The solvent was allowed to evaporate in the air until it became a gel. The resultant gel is transparent and stable and used as a gel electrolyte in solid-state device fabrication.

The electrochemical properties and capacitance measurements of the VO_2 electrodes were studied by cyclic voltammetry (CV) and galvanostatic charge-discharge cycling at different current densities. The specific capacitance C_{sp} was calculated from the charge discharge curves as according to the following equations 1 and 2 respectively for three and two electrode configurations

$$C_{sp} \quad \frac{1}{m}\frac{I}{dV/dt} \tag{1}$$

$$C_{sp} \quad \frac{2}{m}\frac{I}{dV/dt} \tag{2}$$

Gravimetric cell capacitance of the flexible solid state supercapacitor device was calculated using the following equation

$$C_g \quad \frac{1}{M}\frac{I}{dV/dt} \tag{3}$$

Where *I* is the current density during discharge process, *dt* is the discharge time, *dV* is the potential window and *m (= 1 mg)* is the mass of active material in one electrode and *M =2m=2 mg*.

The energy (E) and power densities (P) for the supercapacitors were calculated from charge–discharge curves at different current densities using equations (4) and (5) respectively.

$$E \quad \frac{1}{2}C_{sp} \quad V^2 \tag{4}$$

where 'ΔV' is the potential window of discharge process.

$$P \quad E/t \tag{5}$$

3. Results and Discussions

SEM analysis is used to investigate the morphology of VO_2 and VO_2 /binder/carbon composite. The SEM images of VO_2 exhibit two-dimensional sheet-like morphology, grown in bundles, and the majority of the nanosheets are aligned vertically as shown in **Figure 1 a and b.** The SEM image of the electrode composite of VO_2, carbon and CMC binder is shown in **Figure**

1c. Hydrophilic nature of CMC binder and VO_2 leads to a uniform stable dispersion of VO_2 (inset of **Figure 1c**) with CMC binder and carbon in water. Details of the structural characterizations of VO_2 nanosheets are shown in **Figure S1.**

TEM analysis is used for the structural analysis of the VO_2 nanosheets. TEM images of 2D VO_2 nanosheets are shown in **Figure 2a**. The TEM image shows the ultrathin nanosheets with lateral dimensions ranging from 60 nm to 2 µm. **Figure 2b** shows the high-resolution TEM image displaying the lattice fringes with a spacing of 0.2 nm, which corresponds to the monoclinic VO_2 phase. The scanning transmission electron micrograph (STEM) image of the VO_2 nanosheets is shown in **Figure 2c**. **Figures 2d-f** represents the elemental mapping of the region selected in **Figure 2c**. The images clearly show the uniform distribution of the elements V, O, and C in the nanosheet. The elements V and O originate from VO_2, and the C originates from the oxalic acid which was used to reduce the bulk powder V_2O_5 during the hydrothermal process.

Supercapacitor electrodes are prepared by drop casting of stable suspension -of VO_2 nanosheets, conducting carbon and the CMC binder in water- over carbon paper, as shown in **Figure 3**. The electrochemical performance of the VO_2 electrodes was investigated using cyclic voltammetry and galvanostatic charge-discharge cycling using three electrode configuration. The CV curves obtained at different scan rates show faradaic behavior in the potential range (-0.3V to 1.1 V) studied (**Figure 4a**). The shape remains unchanged at scan rates ranging from 2-50 mV/s with minimal peak shift, indicating efficient electron transfer in the electrodes. The galvanostatic charge-discharge curves at different current densities are shown in **Figure 4b**. A specific capacitance of about 405 Fg^{-1} is achieved for the VO_2 electrode in three electrode configuration in the organic electrolyte (1M $LiClO_4$ in PC) at a constant current density of 1 Ag^{-1}. This value is nearly 1.6 times higher than the specific capacitance reported for V_2O_5 nanosheets in 1M KCl

aqueous electrolyte in our earlier work [61]. The two electrode configuration is more appropriate to study the capacitance as it mimics the design of a real capacitor. Hence, symmetric supercapacitors are constructed using VO_2 electrodes and an organic electrolyte. The CV and CD measurements are conducted, and the results are shown in **Figure 4c and 4d** respectively. The symmetric supercapacitor exhibits specific capacitance values of 230, 217, 192, 172, 154, 128 and 114 Fg^{-1} respectively at scan rates 2, 5, 10, 20, 50, 100 and 200 mV s^{-1}. The specific capacitance value obtained in this study are lower than those reported for VO_2 electrodes in aqueous electrolytes. However, this can be readily explained owing to the higher viscosity and lower conductivity of organic electrolyte PC as compared to water. The specific capacitance values decrease rapidly at higher scan rates and stabilizes at lower scan rates. At lower scan rates and current densities, electrolyte ions in the organic electrolyte get enough time to diffuse from one electrode to another contributing to larger capacitance values.

The variation of capacitance with current density obtained from charge-discharge curves is shown in **Figure S2**, which shows that a specific capacitance of about 170 Fg^{-1} is obtained for the symmetric capacitor at a constant current density of 1 Ag^{-1}. The supercapacitor retains a specific capacitance of 75 Fg^{-1} at a very high current density of 40 Ag^{-1}, indicating reasonably good transport properties of the device. The Ragone plot for the symmetric supercapacitor based on VO_2 electrodes and the liquid organic electrolyte is shown in **Figure 4e**. The energy and power density values in the plot are derived from charge–discharge curves at different current densities. At a constant power density of 25 kW kg^{-1}, the supercapacitor exhibited an energy density of 35 Wh kg^{-1}. At a low power density of 1.4 kW kg^{-1}, the energy density reached as high as 46 W h kg^{-1}, much higher than that reported for VO_2 based aqueous symmetric capacitors[54, 56, 58, 61-64]These results indicate that even though VO_2 based organic symmetric capacitor exhibits lower specific capacitance performance than the aqueous capacitor, the wide operating voltage range of the organic electrolyte system (1.4 V) contributes to the significant enhancement of the energy and power density performance. The long-term cycling stability of the VO_2 based symmetrical supercapacitor is tested using galvanostatic charge-discharge cycling at a constant current density

of 10 Ag^{-1}. The variation of capacitance with cycle number is shown in **Figure 4f**. A sharp increase in the specific capacitance (increase of nearly 6% of the initial capacitance) is observed in the initial 500 cycles, which can be explained as the activation process of the electrode materials. Long charging–discharging process may help electrolyte ions intercalate into the spaces between VO_2 nanosheets, fully utilizing the elective surface area of electrode materials. Due to this Li intercalation enhanced pseudocapacitance, the maximum specific capacitance is achieved at 500^{th} cycle. After that there is a gradual decrease in the capacitance values to next 800 cycles (loss of nearly 10% of the maximum capacitance).The presence of oxygen-containing hydrophilic functional groups and moisture on the surface of VO_2 can be responsible for this degradation in the specific capacitance in organic electrolyte. The specific capacitance becomes quite stable after that (slight decrease with number of cycles). The VO_2 based organic symmetric capacitor could retain nearly 82% of its maximum capacitance (more than 95% of the initial capacitance) even after 6000 charge-discharge cycles.

The charge transfer kinetics of symmetric supercapacitor based on VO_2 electrodes and the liquid organic electrolyte was investigated using the electrochemical impedance spectroscopy in the frequency range of 100 kHz-1 mHz, and the Nyquist plot is shown in **Figure 5a.** The plot shows the semicircle in the high-frequency region and a straight line in the low-frequency region. The X intercept of the Nyquist plot in the high-frequency region gives the value uncompensated resistance of the bulk electrolyte solution (R_s). The diameter of the semi-circle in the high-frequency region corresponding to the charge-transfer resistance (R_{ct}). For the VO_2 based symmetric supercapacitor, The R_s and R_{ct} values obtained from the Nyquist plot are 2.6 and 0.9 Ω respectively. The low value for R_{ct} indicates high conductivity of the VO_2 composite electrodes with excellent electrolyte accessibility. The line at the low-frequency region, making an angle 45° with the real axis, is called the Warburg line resulting from the frequency dependence of ion diffusion in the electrolyte to the electrode interface. Variation of specific capacitance with frequency for symmetric supercapacitor based on VO_2/C/CMC electrodes is shown in **Figure 5b.**

The plot indicates a pseudocapacitive behavior with a continuous increase in the specific capacitance with the decrease in frequency.

Developing energy storage devices which can be integrated into the flexible electronic devices has attracted considerable attention. An essential requirement to develop solid-state flexible energy storage devices is to have a solid-like gel electrolyte which can facilitate ionic conduction in the solid-state device. Fumed silica has been used to form ion gels using ionic liquids[65]. Here, we have developed a slightly different approach to form the fumed silica gel. Instead of using expensive ionic liquids, the liquid electrolyte solution of 1 M $LiClO_4$ in propylene carbonate is used to form the gel with fumed silica. The 1 M $LiClO_4$ solution of propylene carbonate acts as a gelling agent as well as the electrolyte. The resultant fumed silica gel is quite stable and transparent. The CVs of the solid-state symmetrical device fabricated with CMC composite electrodes is shown in **Figure 6a**. The CVs show almost rectangular shape in the gel electrolyte. The charge-discharge characteristics of the solid-state devices at different rates are shown in **Figure 6b.** A specific capacitance of about 145 Fg^{-1} and a gravimetric cell capacitance of 36 Fg^{-1} are achieved at a discharge current density of 1 Ag^{-1}. The decrease in capacitance could be due to the decrease in ion diffusional properties of the gel electrolytes when compared to the liquid electrolytes. The variation of specific capacitance and gravimetric cell capacitance with different current densities for the solid state device is shown in **Figure 6c**. At the high current density of 25 Ag^{-1}, the device retains a specific capacitance of 84 Fg^{-1} and a cell capacitance 21 Fg^{-1}, demonstrating good transport phenomena required for the fast delivery of energy of the gel electrolyte. The flexibility of the solid state device was examined by conducting the CV measurements at different bending angles at a constant scan rate of 50 mV/s and the results are shown in **Figure 6d.** The CVs show negligible change in currents at different bending angles

compared to the flat configuration. The shape of the CVs at different bending angles remains almost the same, demonstrating that the solid-state device can be integrated into flexible platforms. Further, we have connected the three solid-state devices in series to power a red LED. The optical images taken at different time intervals of lighting an LED with the fully charged energy storage devices are shown in **Figure 7a-c.** The solid-state device could power the LED for more than a minute.

4. Conclusions

2D VO_2 nanosheets with high surface area and excellent electrochemical properties were synthesized by the simultaneous exfoliation and reduction of V_2O_5 bulk powder by a hydrothermal route. Flexible supercapacitor electrodes were fabricated by drop-casting water-based suspension containing VO_2 nanosheets, conducting carbon and CMC binder over carbon paper. The symmetric supercapacitor based on VO_2 nanosheet electrodes and liquid organic electrolyte (1M $LiClO_4$ in PC) exhibited an energy density of 46 Wh kg^{-1} at a power density of 1.4 kW kg^{-1} and a constant current density of 1 Ag^{-1}. Flexible solid-state symmetric supercapacitor was also fabricated using organic gel electrolyte and VO_2 nanosheet electrodes which exhibited a specific capacitance of 145 Fg^{-1} and a device capacitance of 36 Fg^{-1} at a discharge current density of 1 Ag^{-1}. The performance of the solid-state device was unaltered at different bending angles and series combination of three such devices could power an LED for more than a minute.

Acknowledgements

Research reported in this publication has been supported by King Abdullah University of Science & Technology (KAUST). Authors thank 'Advanced nanofabricationNanofabrication, Imaging and Characterization Laboratory and 'Analytical Chemistry Core Laboratory' at KAUST. R.B.Rakhi acknowledges the support of Ramanujan Fellowship, Department of Science and Technology (DST), Govt.of India and CSIR-NIIST Thiruvananthapuram, India.

Appendix A. Supplementary data

Supplementary data associated with this article is attached as a separate file.

References

[1] Z. Yang, D. Gao, J. Zhang, Q. Xu, S. Shi, K. Tao, D. Xue, Realization of high Curie temperature ferromagnetism in atomically thin MoS2 and WS2 nanosheets with uniform and flower-like morphology, Nanoscale, 7 (2015) 650-658.
[2] S.-K. Kim, J.J. Wie, Q. Mahmood, H.S. Park, Anomalous nanoinclusion effects of 2D MoS2 and WS2 nanosheets on the mechanical stiffness of polymer nanocomposites, Nanoscale, 6 (2014) 7430-7435.
[3] A.A. Jeffery, C. Nethravathi, M. Rajamathi, Two-Dimensional Nanosheets and Layered Hybrids of MoS2 and WS2 through Exfoliation of Ammoniated MS2 (M = Mo,W), Journal of Physical Chemistry C, 118 (2014) 1386-1396.
[4] M. Thripuranthaka, R.V. Kashid, C.S. Rout, D.J. Late, Temperature dependent Raman spectroscopy of chemically derived few layer MoS2 and WS2 nanosheets, Applied Physics Letters, 104 (2014).
[5] M. Li, A. Zhao, K. Dong, W. Li, J. Ren, X. Qu, Chemically exfoliated WS2 nanosheets efficiently inhibit amyloid beta-peptide aggregation and can be used for photothermal treatment of Alzheimer's disease, Nano Research, 8 (2015) 3216-3227.
[6] K. Gopalakrishnan, S. Sultan, A. Govindaraj, C.N.R. Rao, Supercapacitors based on composites of PANI with nanosheets of nitrogen-doped RGO, BC1.5N, MoS2 and WS2, Nano Energy, 12 (2015) 52-58.
[7] X.-Z. Cui, Z.-G. Zhou, Y. Yang, J. Wei, J. Wang, M.-W. Wang, H. Yang, Y.-J. Zhang, S.-P. Yang, PEGylated WS2 nanosheets for X-ray computed tomography imaging and photothermal therapy, Chinese Chemical Letters, 26 (2015) 749-754.
[8] H. Li, L. Peng, Y. Zhu, X. Zhang, G. Yu, Achieving High-Energy−High-Power Density in a Flexible Quasi Solid-State Sodium Ion Capacitor, Nanoletters, 16 (2016) 5938-5943.
[9] H.S. Li, Y. Zhu, S.Y. Dong, L.F. Shen, Z.J. Chen, X.G. Zhang, G.H. Yu, Self-Assembled Nb2O5 Nanosheets for High Energy-High Power Sodium Ion Capacitors, Chemistry of Materials, 28 (2016) 5753-5760.
[10] S.P.S. Badwal, S.S. Giddey, C. Munnings, A.I. Bhatt, A.F. Hollenkamp, Emerging electrochemical energy conversion and storage technologies, Frontiers in chemistry, 2 (2014) 79-79.
[11] Z. Yu, L. Tetard, L. Zhai, J. Thomas, Supercapacitor electrode materials: nanostructures from 0 to 3 dimensions, Energy & Environmental Science, 8 (2015) 702-730.
[12] J. Yan, Q. Wang, T. Wei, Z. Fan, Recent Advances in Design and Fabrication of Electrochemical Supercapacitors with High Energy Densities, Advanced Energy Materials, 4 (2014).
[13] R.S. Devan, R.A. Patil, J.H. Lin, Y.R. Ma, One-dimensional metal-oxide nanostructures: Recent developments in synthesis, characterization, and applications, Advanced Functional Materials, 22 (2012) 3326-3370.
[14] H. Jiang, J. Ma, C. Li, Mesoporous carbon incorporated metal oxide nanomaterials as supercapacitor electrodes, Advanced Materials, 24 (2012) 4197-4202.
[15] J. Jiang, Y. Li, J. Liu, X. Huang, C. Yuan, X.W. Lou, Recent advances in metal oxide-based electrode architecture design for electrochemical energy storage, Advanced Materials, 24 (2012) 5166-5180.
[16] B. Jin, Q. Yan, Y. Dou, Materials for energy storage and conversion based on metal oxides, Recent Patents on Materials Science, 5 (2012) 199-212.
[17] A.K. Shukla, T. Prem Kumar, Nanostructured electrode materials for electrochemical energy storage and conversion, Wiley Interdisciplinary Reviews: Energy and Environment, 2 (2013) 14-30.

[18] G. Wang, L. Zhang, J. Zhang, A review of electrode materials for electrochemical supercapacitors, Chemical Society Reviews, 41 (2012) 797-828.
[19] C. Wu, F. Feng, Y. Xie, Design of vanadium oxide structures with controllable electrical properties for energy applications, Chemical Society Reviews, 42 (2013) 5157-5183.
[20] S. Devaraj, N. Munichandraiah, Effect of crystallographic structure of MnO2 on its electrochemical capacitance properties, Journal of Physical Chemistry C, 112 (2008) 4406-4417.
[21] P. Kumar Nayak, N. Munichandraiah, Reversible insertion of a trivalent cation onto MnO2 leading to enhanced capacitance, Journal of the Electrochemical Society, 158 (2011) A585-A591.
[22] S. Yang, Y. Gong, Z. Liu, L. Zhan, D.P. Hashim, L. Ma, R. Vajtai, P.M. Ajayan, Bottom-up approach toward single-crystalline VO2-graphene ribbons as cathodes for ultrafast lithium storage, Nano Letters, 13 (2013) 1596-1601.
[23] H. Chen, L. Hu, Y. Yan, R. Che, M. Chen, L. Wu, One-step fabrication of ultrathin porous nickel hydroxide-manganese dioxide hybrid nanosheets for supercapacitor electrodes with excellent capacitive performance, Advanced Energy Materials, 3 (2013) 1636-1646.
[24] D. Guo, X. Yu, W. Shi, Y. Luo, Q. Li, T. Wang, Facile synthesis of well-ordered manganese oxide nanosheet arrays on carbon cloth for high-performance supercapacitors, Journal of Materials Chemistry A, 2 (2014) 8833-8838.
[25] Y. Xie, Y. Dall'Agnese, M. Naguib, Y. Gogotsi, M.W. Barsoum, H.L. Zhuang, P.R.C. Kent, Prediction and Characterization of MXene Nanosheet Anodes for Non-Lithium-Ion Batteries, Acs Nano, 8 (2014) 9606-9615.
[26] M. Huang, Y. Zhang, F. Li, L. Zhang, R.S. Ruoff, Z. Wen, Q. Liu, Self-assembly of mesoporous nanotubes assembled from interwoven ultrathin birnessite-type MnO2 nanosheets for asymmetric supercapacitors, Scientific Reports, 4 (2014).
[27] Y. Huang, Y. Li, Z. Hu, G. Wei, J. Guo, J. Liu, A carbon modified MnO2 nanosheet array as a stable high-capacitance supercapacitor electrode, Journal of Materials Chemistry A, 1 (2013) 9809-9813.
[28] Q. Tang, M. Sun, S. Yu, G. Wang, Preparation and supercapacitance performance of manganese oxide nanosheets/graphene/carbon nanotubes ternary composite film, Electrochimica Acta, 125 (2014) 488-496.
[29] H. Chen, L.F. Hu, M. Chen, Y. Yan, L.M. Wu, Nickel- Cobalt Layered Double Hydroxide Nanosheets for High- performance Supercapacitor Electrode Materials, Advanced Functional Materials, 24 (2014) 934-942.
[30] L. Zhao, J. Yu, W. Li, S. Wang, C. Dai, J. Wu, X. Bai, C. Zhi, Honeycomb porous MnO2 nanofibers assembled from radially grown nanosheets for aqueous supercapacitors with high working voltage and energy density, Nano Energy, 4 (2014) 39-48.
[31] Y. Zhao, P. Jiang, MnO2 nanosheets grown on the ZnO-nanorod-modified carbon fibers for supercapacitor electrode materials, Colloids and Surfaces A: Physicochemical and Engineering Aspects, 444 (2014) 232-239.
[32] J. Jiang, W. Shi, S. Song, Q. Hao, W. Fan, X. Xia, X. Zhang, Q. Wang, C. Liu, D. Yan, Solvothermal synthesis and electrochemical performance in super-capacitors of Co3O4/C flower-like nanostructures, Journal of Power Sources, 248 (2014) 1281-1289.
[33] C.W. Kung, H.W. Chen, C.Y. Lin, R. Vittal, K.C. Ho, Synthesis of Co 3O 4 nanosheets via electrodeposition followed by ozone treatment and their application to high-performance supercapacitors, Journal of Power Sources, 214 (2012) 91-99.
[34] M. Naguib, O. Mashtalir, J. Carle, V. Presser, J. Lu, L. Hultman, Y. Gogotsi, M.W. Barsoum, Two-Dimensional Transition Metal Carbides, Acs Nano, 6 (2012) 1322-1331.
[35] R.B. Rakhi, W. Chen, M.N. Hedhili, D. Cha, H.N. Alshareef, Enhanced rate performance of mesoporous Co3O4 nanosheet supercapacitor electrodes by hydrous RuO2 nanoparticle decoration, ACS Applied Materials and Interfaces, 6 (2014) 4196-4206.

[36] X. Wang, S. Liu, H. Wang, F. Tu, D. Fang, Y. Li, Facile and green synthesis of Co 3O 4 nanoplates/graphene nanosheets composite for supercapacitor, Journal of Solid State Electrochemistry, 16 (2012) 3593-3602.
[37] J. Zhu, L. Cao, Y. Wu, Y. Gong, Z. Liu, H.E. Hoster, Y. Zhang, S. Zhang, S. Yang, Q. Yan, P.M. Ajayan, R. Vajtai, Building 3D structures of vanadium pentoxide nanosheets and application as electrodes in supercapacitors, Nano Letters, 13 (2013) 5408-5413.
[38] L. Cao, J. Zhu, Y. Li, P. Xiao, Y. Zhang, S. Zhang, S. Yang, Ultrathin single-crystalline vanadium pentoxide nanoribbon constructed 3D networks for superior energy storage, Journal of Materials Chemistry A, 2 (2014) 13136-13142.
[39] Z. Chen, V. Augustyn, J. Wen, Y. Zhang, M. Shen, B. Dunn, Y. Lu, High-performance supercapacitors based on intertwined CNT/V 2O 5 nanowire nanocomposites, Advanced Materials, 23 (2011) 791-795.
[40] C.Y. Foo, A. Sumboja, D.J.H. Tan, J. Wang, P.S. Lee, Flexible and Highly Scalable V2O5-rGO Electrodes in an Organic Electrolyte for Supercapacitor Devices, Advanced Energy Materials, (2014).
[41] B.H. Kim, C.H. Kim, K.S. Yang, A. Rahy, D.J. Yang, Electrospun vanadium pentoxide/carbon nanofiber composites for supercapacitor electrodes, Electrochimica Acta, 83 (2012) 335-340.
[42] B.H. Kim, K.S. Yang, D.J. Yang, Electrochemical behavior of activated carbon nanofiber-vanadium pentoxide composites for double-layer capacitors, Electrochimica Acta, 109 (2013) 859-865.
[43] W.F. Mak, G. Wee, V. Aravindan, N. Gupta, S.G. Mhaisalkar, S. Madhavi, High-energy density asymmetric supercapacitor based on electrospun vanadium pentoxide and polyaniline nanofibers in aqueous electrolyte, Journal of the Electrochemical Society, 159 (2012) A1481-A1488.
[44] S.D. Perera, B. Patel, N. Nijem, K. Roodenko, O. Seitz, J.P. Ferraris, Y.J. Chabal, K.J. Balkus Jr, Vanadium oxide nanowire-carbon nanotube binder-free flexible electrodes for supercapacitors, Advanced Energy Materials, 1 (2011) 936-945.
[45] B. Saravanakumar, K.K. Purushothaman, G. Muralidharan, Interconnected V 2O 5 nanoporous network for high-performance supercapacitors, ACS Applied Materials and Interfaces, 4 (2012) 4484-4490.
[46] M. Sathiya, A.S. Prakash, K. Ramesha, J.M. Tarascon, A.K. Shukla, V2O5-anchored carbon nanotubes for enhanced electrochemical energy storage, Journal of the American Chemical Society, 133 (2011) 16291-16299.
[47] G. Wee, H.Z. Soh, Y.L. Cheah, S.G. Mhaisalkar, M. Srinivasan, Synthesis and electrochemical properties of electrospun V2O 5 nanofibers as supercapacitor electrodes, Journal of Materials Chemistry, 20 (2010) 6720-6725.
[48] D. Wei, M.R.J. Scherer, C. Bower, P. Andrew, T. Ryhänen, U. Steiner, A nanostructured electrochromic supercapacitor, Nano Letters, 12 (2012) 1857-1862.
[49] G.P. Nagabhushana, G.T. Chandrappa, Facile solution combustion synthesis of monoclinic VO2: a unique and versatile approach, Journal of Materials Chemistry A, 1 (2013) 11539-11542.
[50] D. Chen, R. Yi, S. Chen, T. Xu, M.L. Gordin, D. Lv, D. Wang, Solvothermal synthesis of V2O5/graphene nanocomposites for high performance lithium ion batteries, Materials Science and Engineering B: Solid-State Materials for Advanced Technology, 185 (2014) 7-12.
[51] J. Cheng, B. Wang, H.L. Xin, G. Yang, H. Cai, F. Nie, H. Huang, Self-assembled V2O5 nanosheets/reduced graphene oxide hierarchical nanocomposite as a high-performance cathode material for lithium ion batteries, Journal of Materials Chemistry A, 1 (2013) 10814-10820.
[52] Y. Li, J. Yao, E. Uchaker, J. Yang, Y. Huang, M. Zhang, G. Cao, Leaf-like V2O5 nanosheets fabricated by a facile green approach as high energy cathode material for lithium-ion batteries, Advanced Energy Materials, 3 (2013) 1171-1175.
[53] L. Liang, H. Liu, W. Yang, Fabrication of VO2(B) hybrid with multiwalled carbon nanotubes to form a coaxial structure and its electrochemical capacitance performance, Journal of Alloys and Compounds, 559 (2013) 167-173.

[54] X. Pan, Y. Zhao, G. Ren, Z. Fan, Highly conductive VO2 treated with hydrogen for supercapacitors, Chemical Communications, 49 (2013) 3943-3945.
[55] W. Sugimoto, T. Shibutani, Y. Murakami, Y. Takasu, Charge storage capabilities of rutile-type RuO2-VO2 solid solution for electrochemical supercapacitors, Electrochemical and Solid-State Letters, 5 (2002) A170-A172.
[56] C. Zhao, J. Cao, Y. Yang, W. Chen, J. Li, Facile synthesis of hierarchical porous VOx@carbon composites for supercapacitors, Journal of Colloid and Interface Science, 427 (2014) 73-79.
[57] H. Zhao, L. Pan, S. Xing, J. Luo, J. Xu, Vanadium oxidesereduced graphene oxide composite for lithium-ion batteries and supercapacitors with improved electrochemical performance, Journal of Power Sources, 222 (2013) 21-31.
[58] H. Wang, H. Yi, X. Chen, X. Wang, One-step strategy to three-dimensional graphene/VO2 nanobelt composite hydrogels for high performance supercapacitors, Journal of Materials Chemistry A, 2 (2014) 1165-1173.
[59] S.T. Senthilkumar, R.K. Selvan, N. Ponpandian, J.S. Melo, Y.S. Lee, Improved performance of electric double layer capacitor using redox additive (VO2+/VO2 +) aqueous electrolyte, Journal of Materials Chemistry A, 1 (2013) 7913-7919.
[60] H. Zhao, L. Pan, S. Xing, J. Luo, J. Xu, Vanadium oxides-reduced graphene oxide composite for lithium-ion batteries and supercapacitors with improved electrochemical performance, Journal of Power Sources, 222 (2013) 21-31.
[61] D.H. Nagaraju, Q. Wang, P. Beaujuge, H.N. Alshareef, Two-dimensional heterostructures of V2O5 and reduced graphene oxide as electrodes for high energy density asymmetric supercapacitors, Journal of Materials Chemistry A, 2 (2014) 17146-17152.
[62] X. Pan, G.F. Ren, M.N.F. Hoque, S. Bayne, K. Zhu, Z.Y. Fan, Fast Supercapacitors Based on Graphene-Bridged V2O3/VOx Core-Shell Nanostructure Electrodes with a Power Density of 1 MW kg(-1), Advanced Materials Interfaces, 1 (2014).
[63] X.J. Ma, W.B. Zhang, L.B. Kong, Y.C. Luo, L. Kang, VO2: from negative electrode material to symmetric electrochemical capacitor, Rsc Advances, 5 (2015) 97239-97247.
[64] L.J. Deng, G.N. Zhang, L.P. Kang, Z.B. Lei, C.L. Liu, Z.H. Liu, Graphene/VO2 hybrid material for high performance electrochemical capacitor, Electrochimica Acta, 112 (2013) 448-457.
[65] S. Wang, B. Hsia, C. Carraro, R. Maboudian, High-performance all solid-state micro-supercapacitor based on patterned photoresist-derived porous carbon electrodes and an ionogel electrolyte, Journal of Materials Chemistry A, 2 (2014) 7997-8002.

Figure captions

1. FESEM images of (a) VO_2 nanosheets, (b) higher magnification image, (c) electrode composite of VO_2, carbon and CMC. Inset of (d) shows the optical image of VO_2 with CMC dispersion solutions along with carbon in water, optical were taken after 45 minutes of their preparation.
2. (a) TEM images showing the nanosheet morphology (b) Higher resolution image showing the lattice fringes, (c) STEM image of nanosheets and (d-f) elemental mapping of vanadium, oxygen and carbon.
3. Schematic of the preparation of the VO_2 nanosheet electrode with CMC binder on graphitized carbon paper.
4. CVs at different scan rates of (a) VO_2/C/CMC electrode and (c) it's symmetric supercapacitor with PC/$LiClO_4$ electrolyte, Charge-discharge characteristics at different current densities of (b) VO_2/C/CMC electrode and (d) its symmetric supercapacitor with PC/$LiClO_4$ electrolyte. (e) ragone plot for VO_2/C/CMC based symmetric supercapacitor. (f) Cycling performance of the symmetric capacitor at a constant current density of $5Ag^{-1}$.
5. (a) Nyquist plot and (b) Variation of specific capacitance with frequency for symmetric supercapacitor based on VO_2/C/CMC electrodes.
6. (a) CVs at different scan rates (b) Charge-discharge characteristics at different current densities and (c) variation of capacitance with current densities for VO_2/C/CMC symmetric supercapacitor device in gel electrolyte, and (d) CVs of solid state device measured at different angles (inset shows the schematic for the measurement of the bending angles and the optical image of the flexible supercapacitor device)
7. Optical images displaying depth of discharge, lighting up the LED using three devices which are connected in series at different intervals of time (a) after 5 s, (b) after 20 s and (c) after 50 s.

Figures

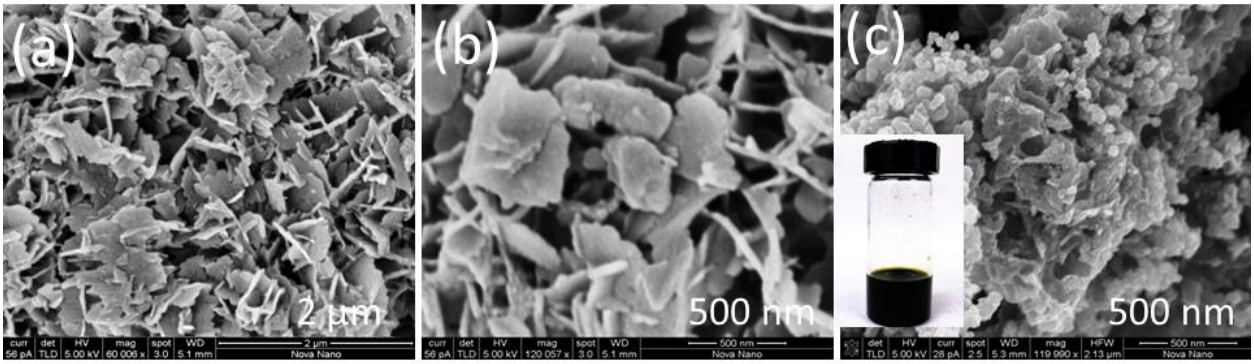

Figure1

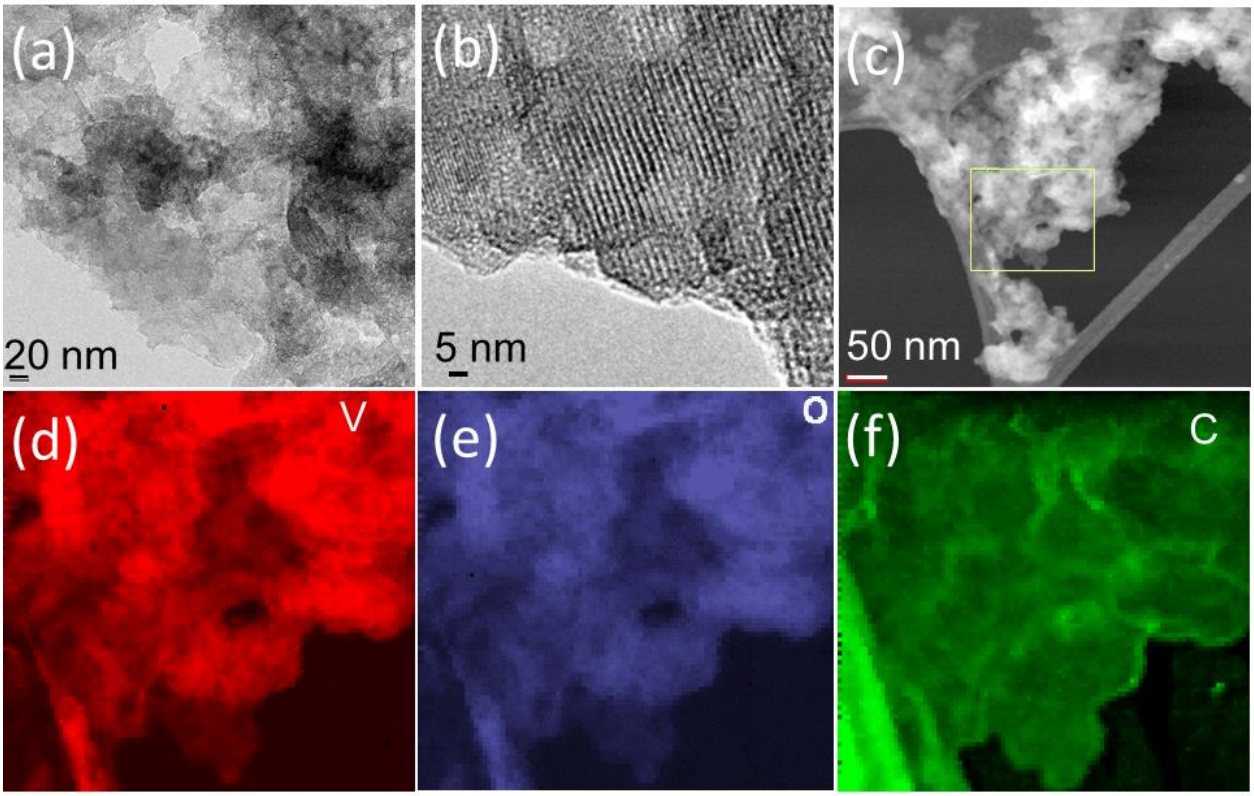

Figure 2

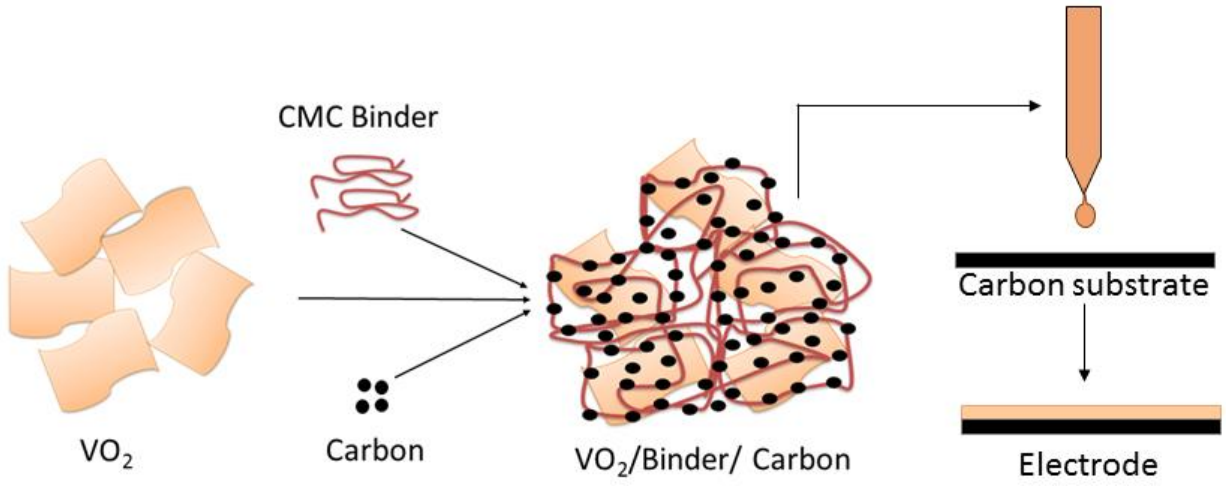

Figure 3

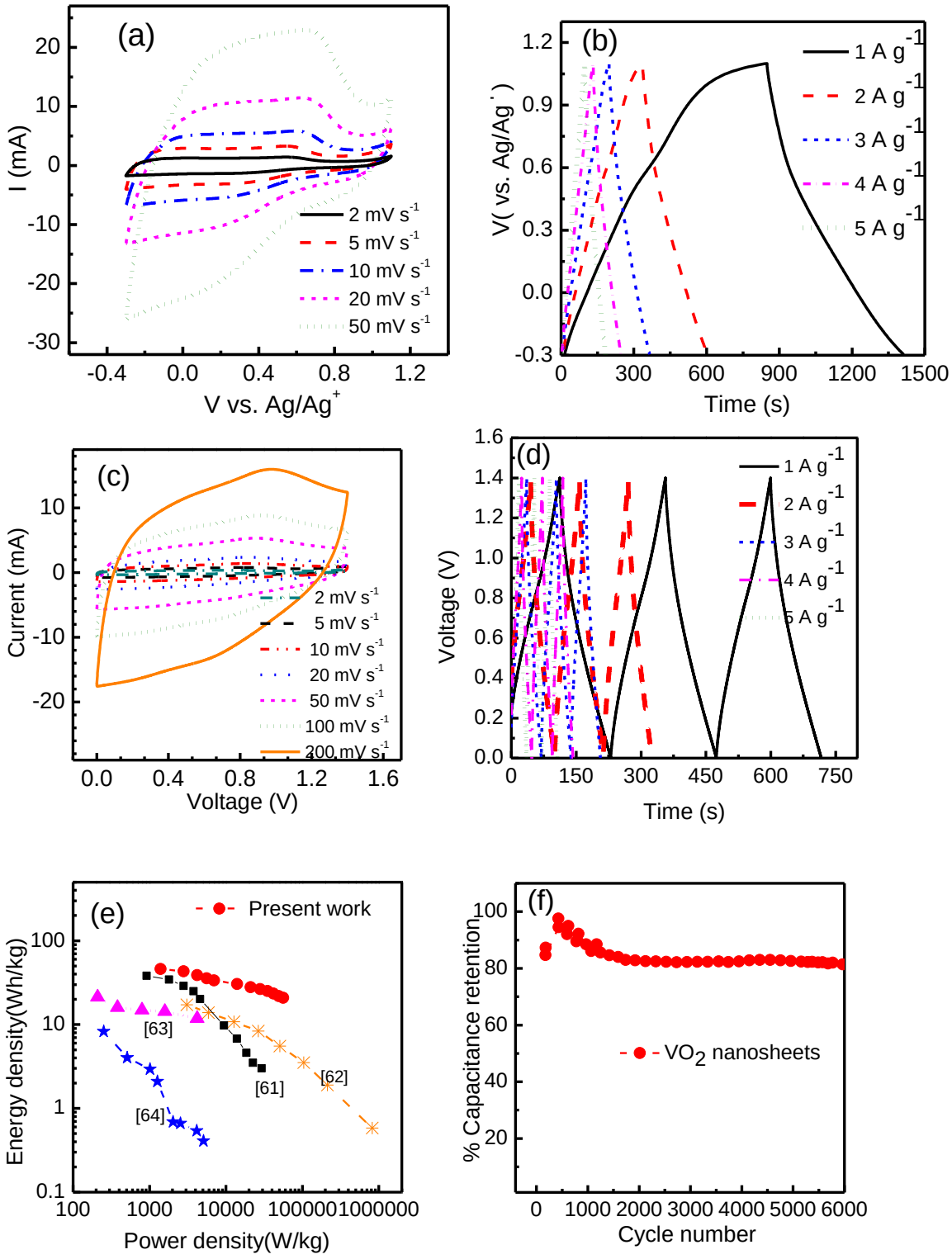

Figure 4

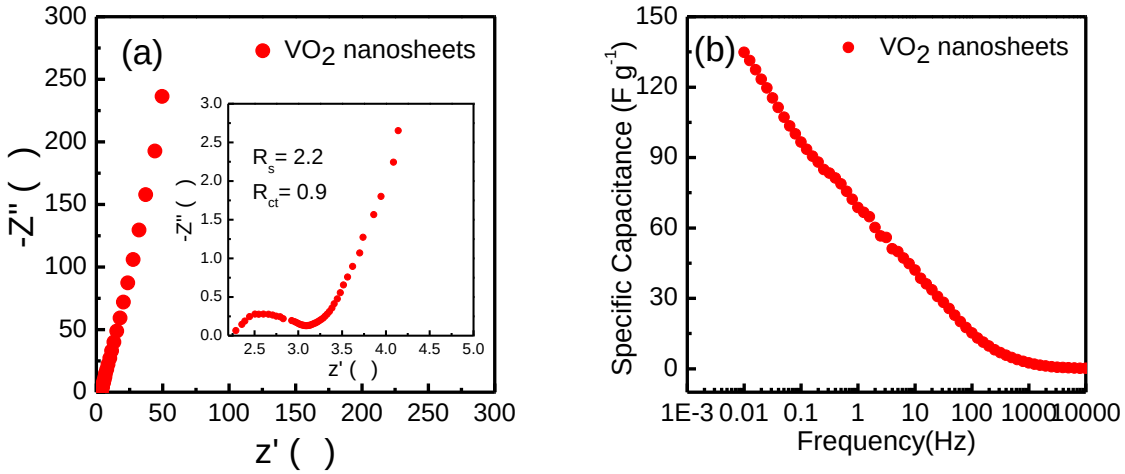

Figure 5

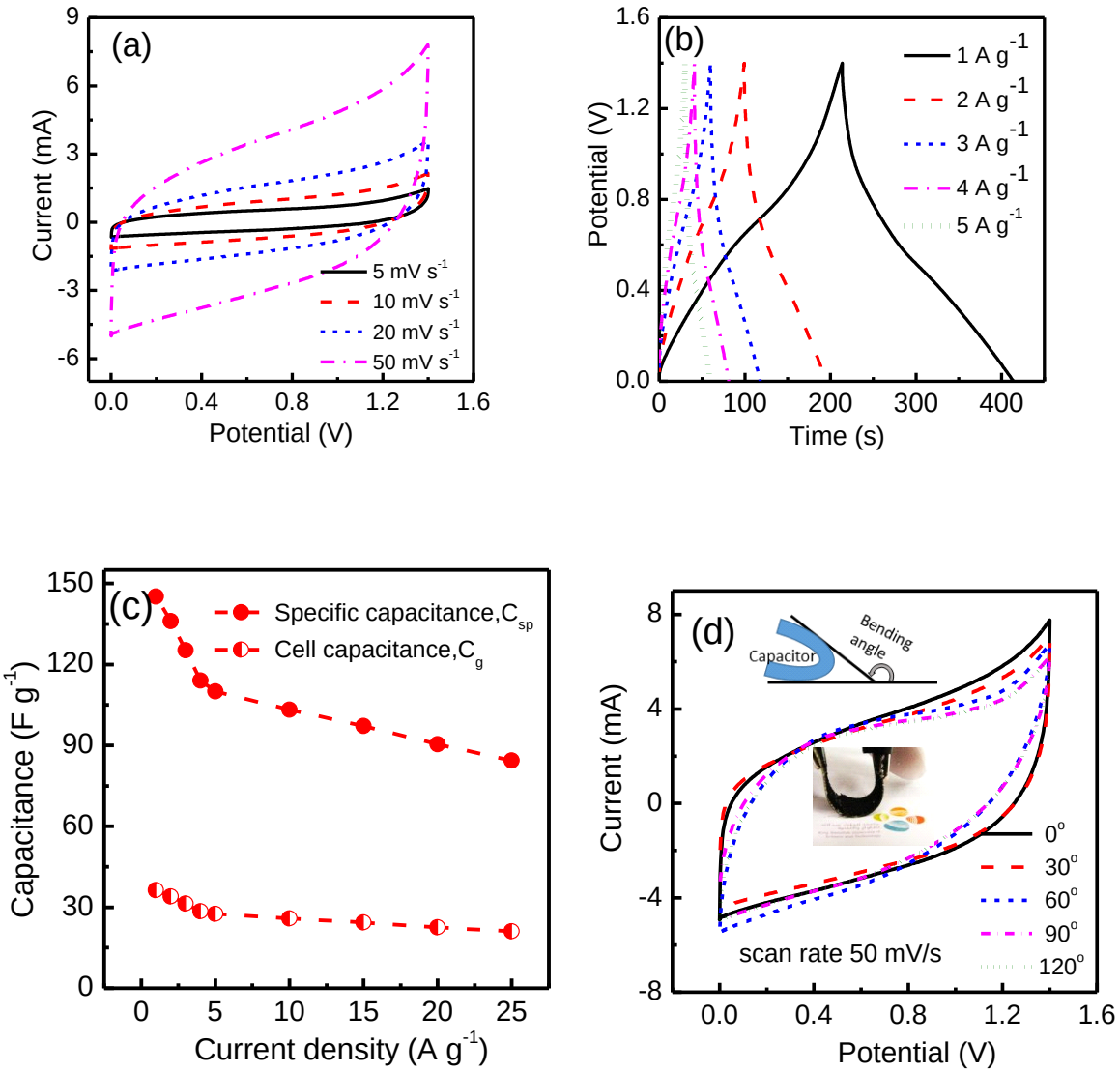

Figure 6

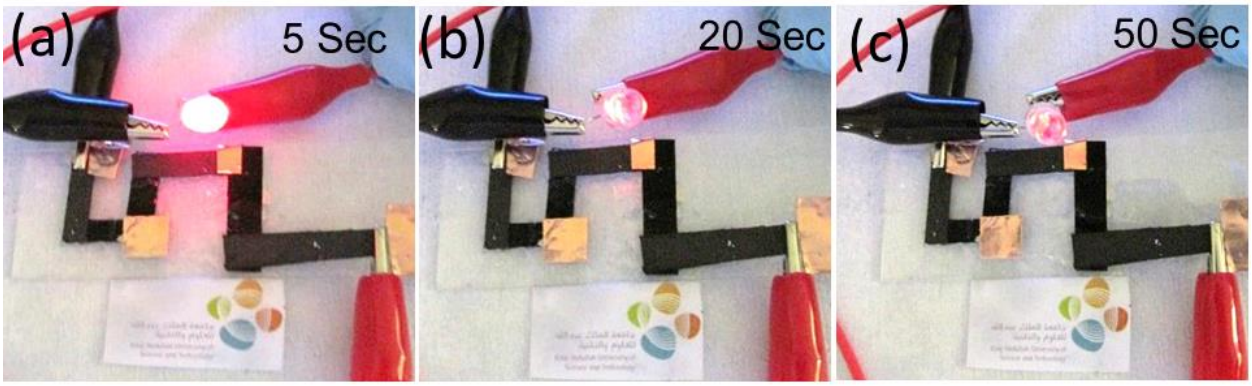

Figure 7